# Formation of Rh Metal Ensembles Facilitating NO Reduction over $Rh/CeO_2$ under Stoichiometric $NO-CO-C_3H_6-O_2$ Reaction

Junya Ohyama,*[a][b] Takumi Nishiyama,[a] and Atsushi Satsuma*[a][b]

**Abstract:** A series of ceria supported rhodium nanoparticles (Rh NPs) having various particle sizes of 2-7 nm was prepared to investigate size effect of Rh NPs on NO reduction under $NO-CO-C_3H_6-O_2$ at stoichiometric conditions. The turnover frequency (TOF) for NO reduction on Rh NPs drastically increased according to their particle size. The strong size dependence of the TOF was attributed to oxidation states of Rh NPs, but not to particle geometries including fractions of surface local sites (e.g., corner, edge, plane) and the surface crystal structures (e.g., Rh(111), (100), etc.) . The variation of the TOF with Rh metal fraction suggested that Rh metal ensembles are highly active species for the NO reduction.

## Introduction

Structural effect of metal nanoparticle (NP) catalysts has been studied to improve catalytic performance and to develop new functions.[1] Metal NPs often show unique structural effect that differs from bulk single crystal surfaces.[2] For instance, Rh and Ru NPs show size dependent catalytic activities for CO oxidation reaction, although Rh and Ru bulk single crystal surfaces do not show structural sensitive activities for the reaction.[2c] The size dependent CO oxidation activities of Rh and Ru catalysts stem from their surface oxidation states or thickness of oxide layer depending on NP size.[2] When metal NPs are supported on metal oxides, metal-support interface sites and unique NP structures and electronic states induced by metal-support interaction can also contribute to catalytic activity.[3]

Improvement of catalyst technology for automotive exhaust gas purification performance has been increasingly demanded to preserve global environment as well as to reduce the usage of the rare metals (e.g., Rh, Pd, Pt) in automotive catalysts. For development of automotive catalyst technology, understanding of structural effect of metal NPs would be helpful since previous studies have suggested that automotive catalyst activity strongly depends on NP structure. [4] In the case of Rh NPs, which are particularly effective for NO reduction in the exhaust gas purification reaction, the previous study by Oh et al. on NO-CO reaction over $Rh/Al_2O_3$ demonstrated that large Rh NPs with 67 nm has 45 times higher turnover frequency (TOF) than small Rh NPs with 1 nm.[4a] The size effect of Rh NPs for NO reduction reaction is not consistent with the structural effect of Rh bulk single crystal surface: Large NPs having high coordination number are more active than small NPs,[5] whereas a bulk single crystal Rh(111) surface is less active than Rh(100), (101), (311) surface having lower coordination number.[6] The size effect of Rh NPs for NO reduction might be related to surface oxidation states under the reaction condition; however, it is not clear because there has been no systematic study on the size effect of Rh NPs on NO reduction reaction.

In the present study, we systematically investigated the size effect of Rh NPs supported on $CeO_2$ for NO reduction reaction under a model gas flow of $NO-CO-C_3H_6-O_2$ at stoichiometric conditions. We synthesized $Rh/CeO_2$ with 2 -7 nm of Rh NPs using various methods including impregnation, Galvanic deposition, and colloid methods. The surface oxidation states of Rh NPs in the catalytic reaction conditions was investigated using X-ray photoelectron and CO adsorption IR spectroscopies to reveal the origin of strong size dependent catalytic activity of $Rh/CeO_2$ for the NO reduction reaction.

## Results and Discussion

We prepared $Rh/CeO_2$ catalysts using various methods including impregnation ($Rh/CeO_2$-I), Galvanic deposition ($Rh/CeO_2$-G),[7] colloid method ($Rh/CeO_2$-C).[8] The $Rh/CeO_2$-C catalysts were prepared using different three Rh nanocolloid solutions prepared in different solvents ($Rh/CeO_2$-C1, -C2, -C3). The preparation procedures are described in the experimental section below. The Rh loadings determined by X-ray fluorescence (XRF) spectroscopy were 1wt% (Table 1). Besides, the catalysts did not show residual Cl and N species on X-ray photoelectron spectra (Figure S1).

The sizes of Rh NPs of the prepared catalysts were measured by $H_2$ pulse adsorption at low temperature on the assumption of hemi-spherical particles.[9] As presented in Table 1, the catalysts have different sizes of Rh NPs in the range of 2-7 nm. The particle sizes of $Rh/CeO_2$-I and -G were also evaluated using CO pulse adsorption technique (Table 1), and were almost the same as those evaluated using $H_2$ pulse adsorption technique. For the particle size analysis, transmission electron microscopy (TEM) is usually helpful; however, TEM observation did not allow us to evaluate the size of Rh NPs on $CeO_2$ appropriately, since Rh species did not show enough contrast against $CeO_2$. Instead, we observed $Rh/CeO_2$-I and -G using STEM-EDX (Figure S2), and confirmed highly dispersed Rh species on $Rh/CeO_2$-I and 2-5 nm of Rh nanoparticles on $Rh/CeO_2$-G. On the other hand, the sizes of the colloidal Rh NPs,

[a] Dr. J. Ohyama, Ms. Y. Zhang, Mr. J. Ito, Prof. A. Satsuma
Graduate School of Engineering
Nagoya University
Furo-cho,Chikusa-ku, Nagoya 464-8603, Japan
E-mail: ohyama@apchem.nagoya-u.ac.jp (J.O.)
satsuma@apchem.nagoya-u.ac.jp (A.S.)
[b] Dr. J. Ohyama, Prof. A. Satsuma
Elements Strategy Initiative for Catalysts and Batteries (ESICB)
Kyoto University
*Katsura, Kyoto 615-8520, Japan*

Supporting information for this article is given via a link at the end of the document.

which are the precursors of the Rh/$CeO_2$-C catalysts, were evaluated using TEM observation (Figure S3). The order of size of colloidal Rh NPs was consistent with that of corresponding Rh/$CeO_2$-C evaluated based on $H_2$ adsorption (Table 1). Since the sizes evaluated by CO adsorption, TEM, and STEM-EDS are consistent with those evaluated by $H_2$ chemisorption method, we use the Rh NP size evaluated by $H_2$ adsorption in the following discussion on size effect of Rh NPs on NO reduction.

We performed NO reduction reaction under NO-CO-$C_3H_6$-$O_2$ using the Rh/$CeO_2$ catalysts. The reaction conditions are stoichiometric and the reaction formula is as follows:

1000 ppm NO + 4000 ppm CO + 1000 ppm $C_3H_6$ + 6000 ppm $O_2$ → 500 ppm $N_2$ + 7000 ppm $CO_2$ + 3000 ppm $H_2O$

The gas concentrations are based on volume and balanced by Ar. Figure 1(a) shows NO conversion as a function of reaction temperature over the series of Rh/$CeO_2$ catalysts under the stoichiometric NO-CO-$C_3H_6$-$O_2$ flow of 60 mL $min^{-1}$. The simultaneously obtained CO and $C_3H_6$ conversions are also presented in Figure 1. According to the literature,[10] NO reduction on Rh catalysts proceeds with dissociative adsorption of NO, formation of $N_2$ by coupling of two N atoms on Rh surface, and removal of the adsorbed O atoms by reductants such as CO and $C_3H_6$. In the case of the reaction over all Rh/$CeO_2$, CO oxidation proceeded prior to $C_3H_6$ oxidation and NO reduction (Figure 1), probably due to fast CO oxidation on Rh-$CeO_2$ interface.[3a, 11] Since the reaction over Rh/$CeO_2$ catalysts showed fast consumption of CO, the reductants for the surface adsorbed O atoms are considered to be $C_3H_6$ and/or its partially oxidized compounds. To confirm the NO reduction mainly by $C_3H_6$ species, we further performed NO-$C_3H_6$-$O_2$ and NO-CO-$O_2$ reactions using Rh/$CeO_2$ catalysts (Figures S5 and S6). As a result, the NO reduction behavior under the NO-$C_3H_6$-$O_2$ reaction was in good agreement with that under the NO-CO-$C_3H_6$-$O_2$ reaction, but that under the NO-CO-$O_2$ was not. The result confirms that $C_3H_6$ mainly functions as a NO reducing agent in the NO-CO-$C_3H_6$-$O_2$ reaction over Rh/$CeO_2$ catalysts.

Note that NO conversion on Rh/$CeO_2$-G and -C catalysts started from and completed at lower temperature than that on Rh/$CeO_2$-I. Since the Rh/$CeO_2$-G and -C have larger Rh NPs than Rh/$CeO_2$-I, it is expected that large Rh NPs have highly active species for the NO reduction.

**Table 1.** Rh loading, dispersion, and particle size of the catalysts prepared in this study.

| Catalyst [a] | Loading (wt%) [b] | Dispersion (%) | Size (nm) |
|---|---|---|---|
| Rh/$CeO_2$-I | 0.96 | 52 [c], 63 [d] | 2.1 [c], 1.8 [d] |
| Rh/$CeO_2$-G | 1.03 | 36 [c], 47 [d] | 3.1 [c], 2.5 [d] |
| Rh/$CeO_2$-C1 | 0.99 | 35 | 3.1 [c], 2.8 [e] |
| Rh/$CeO_2$-C2 | 0.97 | 20 | 5.6 [c], 3.5 [e] |
| Rh/$CeO_2$-C3 | 1.02 | 17 | 6.6 [c] 4.2 [e] |

[a] Rh/$CeO_2$-I was prepared by the impregnation method, Rh/$CeO_2$-G by the Galvanic deposition, Rh/$CeO_2$-C1, -C2, and -C3 by the colloid method. [b] Determined from XRF. [c] Calculated from $H_2$ adsorption amount. [d] Calculated from CO adsorption amount. [e] Average size of colloidal Rh NPs determined using TEM observation (Figure S2) before deposition on $CeO_2$.

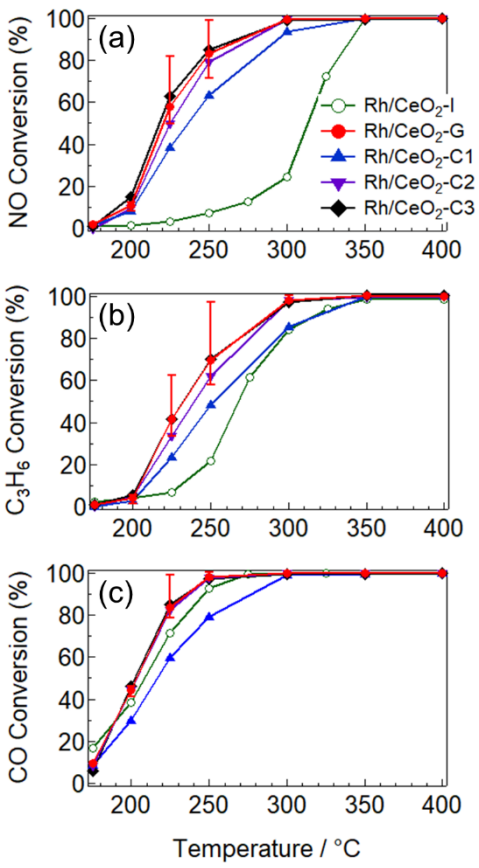


**Figure 1.** (a) NO, (b) CO, and (c) $C_3H_6$ conversion on the series of Rh/$CeO_2$ catalysts under a stoichiometric NO-CO-$C_3H_6$-$O_2$ flow. Rh/$CeO_2$-I (green open circle), -G (red closed circle), -C1 (blue triangle), -C2 (purple inverted triangle), and -C3 (black diamond). The results of Rh/$CeO_2$-G shows the error by repeated experiment for three times. The reaction conditions are described on experimental section.

For accurate analysis and comparison of the kinetics on the Rh catalysts, we need to obtain low reactant conversion (< ca. 20%) at an identical reaction temperature on all catalysts. Thus, the catalyst amounts (Rh/$CeO_2$-I: 20 mg; the others: 5 mg) and the reaction temperature (210˚C) were adjusted to obtain NO conversion of 1-12%. Then, the turnover frequency (TOF) from the NO conversion at 210˚C and the number of Rh surface atom determined by $H_2$ adsorption: TOF ($s^{-1}$) = NO reduction rate at 210˚C (mol $s^{-1}$) / Rh surface atom (mol). In Figure 2, the TOF was plotted against the size of Rh NPs. The TOF increases with the size of Rh NPs, indicating that larger Rh NPs have highly active species for the NO reduction. The result is consistent with the previous reports on supported Rh catalysts for NO-CO reaction.[4a, 12] Note that the size dependency of the

TOF (Figure 2) does not follow the fraction of surface local sites (corner, edge, and plane) of Rh NPs with a model structure, e.g., cuboctahedron.[5] One might consider that the surface structure contributes to the TOF. Actually, previous studies on Rh single crystal surface have demonstrated that lower coordinated Rh surface such as Rh(100), (110) and (311) have higher catalytic activity than Rh(111);[6] however, the Rh surface structure cannot account for the size dependent catalytic activity of Rh NPs, because Rh NPs show the oposit trend to Rh single crystal surfaces, and small Rh NPs with low coordinated sites at high fraction are less active. It is suggested that the other factor(s) than particle surface geometries determine the catalytic activity of Rh NPs for the NO reduction.

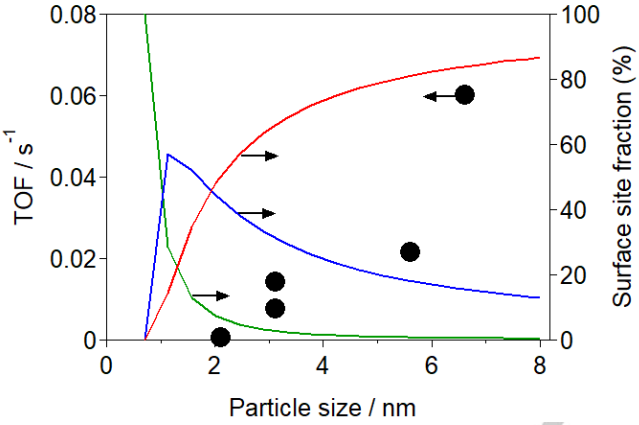


**Figure 2.** Size dependence of TOF on RhNP size (black closed circle). Calculated fraction of surface sites on cuboctahedron models of RhNPs with various particle sizes: plane sites in red, edge in blue, and corner in green. The fraction of corner, edge, and plane atoms on Rh particles were calculated using the equations of the previous report[5] with modification of atomic radius with Rh one (2.68 Å)

Previous studies have suggested that the catalytic activity of Rh NPs can be strongly affected by their oxidation states, which can be varied with the size of Rh NPs.[2a, 2b, 2d] Thus, we evaluated the fractions of Rh metal and oxide of the Rh catalysts using XPS. Figure 3 shows the Rh 3d XP spectra of the various Rh catalysts which were treated under the reaction gas flow at 250˚C. The spectra were well fitted with two curves for Rh $3d_{5/2}$ peak at ca. 307 eV, and other two curves for Rh $3d_{3/2}$ at ca. 312-314 eV. The separated two peaks of Rh $3d_{5/2}$ at ca. 307 and 309 eV are attributable to Rh metal and oxide, respectively.[13] The well fitted curves were Gaussian functions, although XPS profiles should be fitted with Voigt (Gaussian-Lorentzian) functions in principle, since they come from inherent photoemission (Lorentzian function) and instrument factor (Gaussian function). It is possible that the deconvoluted Gaussian peaks contain minor peaks due to slightly differently charged Rh species such as $Rh^{0+\delta}$ and $Rh^{0-\delta}$ in the Rh metal peak and $RhO_{x+\delta}$ and $RhO_{x-\delta}$ in the Rh oxide peak. In the present study, we simply evaluated Rh metal fraction from the area of two Gaussian functions of Rh metal and Rh oxide without considering minor charge variation in Rh metal and $RhO_x$. Figure 4 presents a plot of the TOF against the Rh metal fraction. The TOF drastically increases with the fraction of Rh metal species, suggesting that the fraction of Rh metal strongly contributes to the catalytic activity. The strong dependency of TOF on Rh metal fraction might suggests that neighboring $Rh^0$ atoms enhance catalytic activity for the NO reduction.

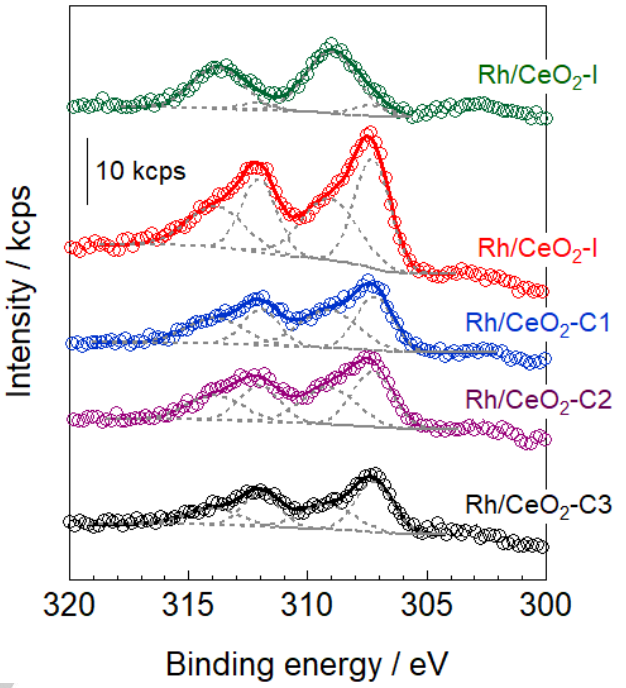


**Figure 3.** Rh 3d XP spectra of the various Rh catalysts after pretreatment under $H_2$ for 10 min, $O_2$ for 10 min at 450˚C, and NO-$C_3H_6$-CO-$O_2$ reaction gas at 250˚C for 30 min. Experimental data: open circles, fitting results: solid lines, Gaussian functions: gray dashed lines.

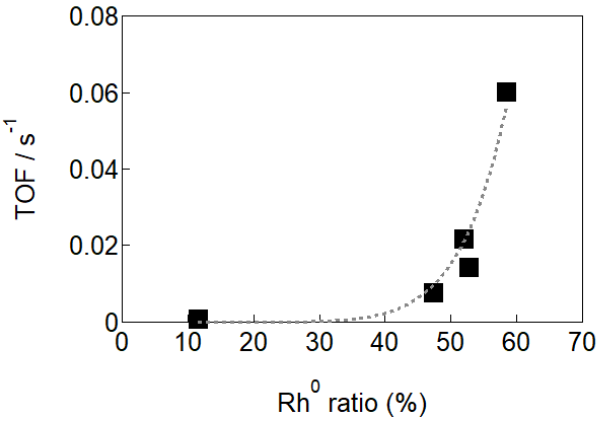


**Figure 4.** Plot of the TOF against the Rh metal fraction determined by the Rh 3d XPS.

The Rh 3d XP spectra contain information about Rh species beneath NP surface (~ 1 nm).[14] In other words, we cannot confirm the oxidation states of Rh species at outermost surface of particles from the Rh 3d XP spectral analysis. To evaluate Rh metal fraction at outermost surface of Rh NPs, we utilized CO adsorption IR spectroscopy.

Figure 5 shows the CO adsorption IR spectra of the Rh catalysts treated under NO-CO-$C_3H_6$-$O_2$ gas flow at 250˚C. According to the literature, the bands observed at 2100-2070 and 2030-2010 $cm^{-1}$ are assignable to germinal dicarbonyl (twin CO) on $Rh^+$, and the bands at 2070-2030 $cm^{-1}$ to linearly adsorbed CO on $Rh^0$.[4c, 12-13, 13d, 15] $Rh/CeO_2$ with larger Rh particles presented the linear CO on $Rh^0$ at higher relative intensity compared to the twin CO on oxidized Rh. It is suggested that larger Rh NPs have higher $Rh^0$ fraction. The result is consistent with the XPS analysis. Another band at 1910-1900 $cm^{-1}$, which is clearly observed on the spectra of $Rh/CeO_2$-I and -G, is assignable to bridge CO on $Rh^0$ or on Rh-Ce interface.[4c, 13a, 13d, 15i-k] Since these catalysts showed relatively small band intensity of linearly adsorbed CO on $Rh^0$, and also the XPS analysis indicated that the $Rh^0$ fractions of these samples are relatively low, we assumed that the bridge CO band on $Rh/CeO_2$-I and -G are due to bridge CO adsorption on the interface between Rh oxide speciess and $CeO_2$.[13d] It should be also mentioned that the bridge CO was hardly observed on $R/CeO_2$-C samples. The catalyst preparation using colloidal method might form less Rh-Ce interface than the other methods. On the basis of above band assignment, we evaluated $Rh^0$ fractions using the band areas (Figure S4) and the reported extinction coefficients:[15i-k, 16] $X_{Rh0} = (A_{linear}/\varepsilon_{linear})/(A_{linear}/\varepsilon_{linear} + A_{twin}/\varepsilon_{twin} + A_{bridge}/\varepsilon_{bridge})$, where $X_{Rh0}$ is $Rh^0$ fraction; $A_{linear}$, $A_{twin}$, and $A_{bridge}$ are the band areas due to linear, twin, and bridge CO adsorption, respectively; $\varepsilon_{linear}$, $\varepsilon_{twin}$, and $\varepsilon_{bridge}$ are the respective extinction coefficients. The value of $\varepsilon_{twin}$ was quoted from the previous report by Rasband et al. ($\varepsilon_{linear}$ = 130 ± 50 $cm^{-1}$). For $\varepsilon_{linear}$ and $\varepsilon_{bridge}$, different values have been reported,[15i-k] thus, we used the averaged ($\varepsilon_{linear}$ = 24 $cm^{-1}$, $\varepsilon_{bridge}$ = 78 $cm^{-1}$), minimum ($\varepsilon_{linear}$ = 11 $cm^{-1}$, $\varepsilon_{bridge}$ = 36 $cm^{-1}$), and maximum values ($\varepsilon_{linear}$ = 42 $cm^{-1}$,$\varepsilon_{bridge}$ = 137 $cm^{-1}$) for the calculation. Figure 6 presents a plot of the TOF against the $Rh^0$ fraction evaluated from the IR bands. The TOF increases with the surface $Rh^0$ fraction, indicating that surface Rh metal species is highly active for the NO reduction.

We conducted a regression analysis of the plot in Figure 6, which indicated that the TOF increases with ca. 5$^{th}$ power of the Rh metal fraction at outermost surface of Rh NPs. The strong dependency of TOF on the surface $Rh^0$ fraction suggests that neighboring $Rh^0$ atoms cause high NO-reduction activity. On the basis of the reaction mechanism,[10] NO reduction on Rh catalysts starts from dissociative adsorption of NO, for which adjacent two adsorption sites would be required. It should be also taken into consideration that $C_3H_6$ species act as reductants for the remaining O atoms on Rh surface. In line with the previous report on Pt catalysts, the remaining O atoms will react with $C_3H_6$ species adsorbed on neighboring $Rh^0$ surface atoms to regenerate the active sites for NO adsorption.[10f] From this perspective, a probability of forming a $Rh^0$ ensemble can be related to the catalytic activity. Since the 5$^{th}$ power of $Rh^0$ fraction is relevant to a probability of forming an ensemble composed of five $Rh^0$ atoms, we propose that retention of such $Rh^0$ ensembles or their easy formation during the reaction would be the key to enhancement of the catalytic activity of Rh catalysts for NO reduction in stoichiometric NO-CO-$C_3H_6$-$O_2$ conditions.

We also calculated the TOF normalized by $Rh^0$ surface atoms under the reaction conditions at 250°C (denoted as $TOF_{Rh0}$). The number of $Rh^0$ surface atoms under the reaction conditions at 250°C was calculated from the total number of Rh surface atoms (determined by $H_2$ adsorption after $H_2$ reduction pretreatment) and the surface $Rh^0$ fraction (determined by the CO adsorption IR after the treatment under the NO-CO-$C_3H_6$-$O_2$ reaction conditions). Figure 7 shows the dependence of $TOF_{Rh0}$ on Rh particle size. The $TOF_{Rh0}$ increased with an increase in particle size, supporting that surroundings of a $Rh^0$ surface atom affect the NO reduction activity. In other words, $Rh^0$ ensembles lead to high activity for NO reduction.

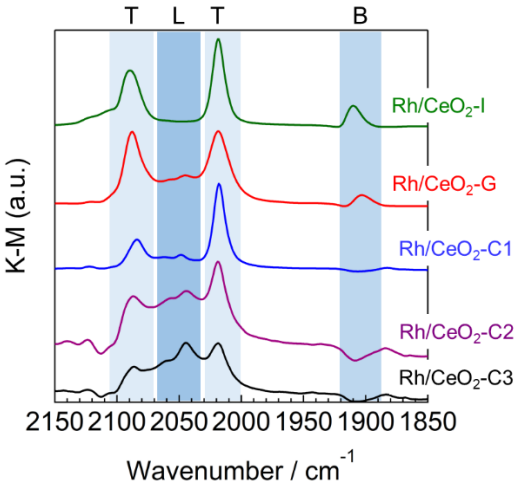


**Figure 5.** FT-IR spectra of CO adsorbed on the various Rh catalysts after treatment under the reaction gas flow at 250˚C for 30 min. L: Linear CO; T: Twin CO; B: Bridge CO.

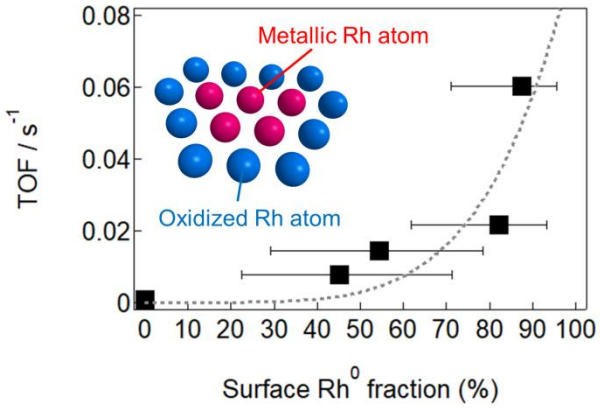


**Figure 6.** Plot of the TOF against the Rh metal fraction determined from the CO adsorption IR spectra. Gray dotted line is the result of regression analysis: $y = 6.0 \times 10^{-12} x^{5.1}$. The illustration is a possible model of highly active Rh metal surface ensemble.

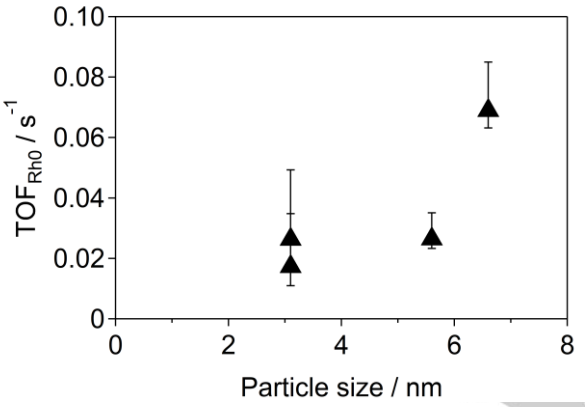


**Figure 7.** Particle size dependence of turnover frequency calculated from number of $Rh^0$ surface atoms ($TOF_{Rh0}$). The errors of $TOF_{Rh0}$s were calculated from the surface $Rh^0$ fraction.

We have demonstrated that Rh metal ensembles are highly active species for NO reduction. As the particle becomes larger, the formation probability of the Rh ensemble increases, and the catalytic activity per surface Rh atom increases. This result would be useful for catalyst design; however, we cannot necessarily propose that simple growth of Rh NPs is not an effective strategy for reduction of Rh usage because the particle growth causes an increase of inside Rh atoms not used for the reaction. Other morphologies that differ from usual NP structures would be needed for formation of highly active Rh metal ensembles at high atomic utilization efficiency. The importance of particle morphology might be shown by the difference of the TOFs between $Rh/CeO_2$-G and -C1 (Table S1). These two catalysts have different TOFs, although their particle sizes were almost the same. The difference in the TOF is accounted for by $Rh^0$ fraction, and the difference in $Rh^0$ fraction between $Rh/CeO_2$-G and –C1 can be derived from morphology of Rh nanoparticles. Actually, the bridge CO species was observed on the CO adsorption IR spectrum of $Rh/CeO_2$-G, but hardly on $Rh/CeO_2$-C1. Since Galvanic deposition method can form thin-layered metal structure,[7b, 7e] $Rh/CeO_2$-G might have a raft-like structure with Rh terrace sites at higher fraction compared to $Rh/CeO_2$-C1 prepared from spherical colloidal Rh NPs. In line with this, extended thin metal layers such as plate are expected to be reasonable morphologies for improvement of Rh catalysts,[7e, 17] since Rh species on plane sites preserve metallic state compared to lower coordinated ones such as corner and edge atoms on a conventional NP structure.

## Conclusions

The particle size dependence of Rh NPs for NO reduction under stoichiometric NO-CO-$C_3H_6$-$O_2$ reaction was investigated using $CeO_2$ supported Rh NPs of 2-7 nm prepared by various methods including impregnation, Galvanic deposition, and colloid methods. The TOF drastically increased with the particle size of Rh NPs. The size dependence was not accounted for by fractions of surface local sites of corner, edge, plane, or by the surface crystal structures. It is suggested that the oxidation states of Rh NPs are responsible for the NO reduction activity. Based on the results of Rh 3d XPS and CO adsorption FT-IR spectral analyses for $Rh/CeO_2$ treated under the reaction conditions, it was indicated that Rh metal species leads to high activity for the NO reduction. The dependence of the TOF on the surface Rh metal fractions suggested that Rh metal ensembles are highly active species for the NO reduction.

## Experimental Section

**Materials.** $CeO_2$ was obtained from Daiichi Kigenso Kagaku Kogyo Co., LTD. (107 $m^2$ $g^{-1}$ of specific surface area). $CeO_2$ powder was calcined at 500˚C for 3 h before use. Rh powder was purchased from Mitsuwa. The other chemicals were purchased from Kishida Chemical Co., Ltd.

**Catalyst preparation.** 1wt% $Rh/CeO_2$ catalysts were prepared by the following four methods.

i) Impregnation method: 495 mg of $CeO_2$ and 8 mL of 6.07 mM $RhCl_3$ aq. was added to 50 mL of water and stirred at r.t. for 1 h. The aqueous suspension was then evaporated at 60˚C. The resulting powder was dried at 80˚C overnight, and calcined at 300˚C at 3h under air.

ii) Galvanic deposition method [7]: 495 mg of $CeO_2$ was treated under a 100 mL $min^{-1}$ of $H_2$ flow at 500˚C for 30 min in a 100 mL round-bottomed flask. After cooling to r.t. under $H_2$ flow, the flask was purged with 100 mL $min^{-1}$ of $N_2$ flow for 10 min. To the reduced $CeO_2$ (purple color), 8 mL of water was added, and then 8 mL of $RhCl_3$ aq. (6.07 mM) was injected for 5 s under stirring. After stirring for 15 min, the suspension was centrifuged to give a solid. The solid was washed twice with 40 mL of water, and dried at 80˚C overnight.

iii) Colloid method [8]: 5.43 mL of $RhCl_3$ aq. (Rh 0.033 mmol) and polyvinylpryrrolidone (PVP) were added to the following three solvents to obtain three kinds of RhNPs: methanol-water (25/25 mL/mL); ethanol (25 mL); ethanol-water (25/25 mL/mL). The solutions were heated under

stirring and reflux at 85˚C in the case of methanol-water solution, and at 100˚C in the case of ethanol containing solutions. After the solution was cooled to to r.t., 336.0 mg of $CeO_2$ was added to each solution. The suspensions were stirred for 1 h, and then evaporated at 50˚C. The resulting solids were dried at 80˚C and calcined at 500˚C for 1 h.

The $Rh/CeO_2$ catalyst prepared by the impregnation method: $Rh/CeO_2$-I; the catalyst prepared by the Galvanic deposition: $Rh/CeO_2$-G; the three catalysts prepared by the colloid method: $Rh/CeO_2$-C1, -C2, and -C3.

**Catalytic test.** The catalysts were pretreated under $O_2$ flow (40 mL $min^{-1}$) at 450˚C for 10 min, under Ar for 10 min, and then under $H_2$ flow (40 mL $min^{-1}$) at 450˚C for 10 min. After cooling to 175˚C under Ar flow, catalytic reaction was performed on a conventional fixed-bed flow reactor at atmospheric pressure with 17.5 mg of catalyst inside a Pyrex glass tube under reaction gas flow (60 mL $min^{-1}$) containing 1000 ppm of NO, 4000 ppm of CO, 1000 ppm of $C_3H_6$, 6000 ppm of $O_2$, and balance Ar (GHSV = 140000 $h^{-1}$). The reaction temperature was increased stepwise from 175 to 450˚C. The outlet gas concentrations were analyzed using $NO_x$ and $CO/CO_2$ analyzer (Horiba VA3000), and recorded at steady state after 30min for each temperature. To determine the TOF from low NO conversion at an identical temperature, the catalyst amount and the reaction temperature were adjusted: 5 mg of $Rh/CeO_2$-G and -C, and 20 mg of $Rh/CeO_2$-I were used at 210°C of the reaction temperature.

**Characterization.** The loadings of $Rh/CeO_2$ catalysts were determined by XRF (Rigaku, EDXL-300). $H_2$ pulse and CO pulse measurement was performed on a BELCAT-B (MicrotracBEL) equipped with a thermal conductivity detector. The catalysts (50 mg) were treated at 450˚C under $O_2$ for 10 min, He for 5 min, $H_2$ for 10 min, and then He for 15 min (flow rate: 50 mL $min^{-1}$). The catalysts were cooled under He to 0˚C using a cryostat (MicrotracBEL, CATCryo) for $H_2$ adsorption. For CO adsorption measurement, after the same pretreatment as the $H_2$ adsorption measurement, $CO_2$ gas was flowed at 50˚C to avoid CO oxidation and adsorption on $CeO_2$, and then CO adsorption was carried out at 50˚C. Rh metal dispersions and particle sizes of the catalysts were calculated from the Rh loading and $H_2$ and CO adsorption amounts assuming spherical shape of Rh NPs

Transmission electron microscope images and energy dispersive spectral images were obtained on a JEOL JEM-2100F at 200 kV of accelerating voltage.

X-ray photoelectron spectra (XPS) of Rh 3d region were taken on a JPS-9000MC system (JEOL Ltd.) using Mg *Kα* radiation. Binding energy was calibrated using C1s peak at 284.6 eV. The catalysts were pretreated under 10% $O_2$/Ar for 10 min, 10% $H_2$/Ar for 10 min at 450˚C, and cooled to 250˚C under Ar. Then, the catalysts were treated under the reaction gas (1000 ppm of NO, 4000 ppm of CO, 1000 ppm of $C_3H_6$, 6000 ppm of $O_2$, and balance Ar) at 250˚C for 30 min.

Diffusion reflectance infrared Fourier transform (DRIFT) IR 0spectra of CO adsorbed on the catalysts were taken on a JASCO FT/IR-6100 (JASCO Co.) with a MCT detector. The catalysts were treated under 10% $O_2$/Ar for 10 min, 10% $H_2$/Ar for 10 min at 450˚C, and then cooled to 250˚C under Ar. The catalysts were further treated under the reaction gas (1000 ppm of NO, 4000 ppm of CO, 1000 ppm of $C_3H_6$, 6000 ppm of $O_2$, and balance Ar) at 250˚C for 30 min, and under a CO probe gas of 1% CO/Ar at 50˚C for 15 min. After purging with Ar for 15 min, DRIFT spectra of CO adsorbed on the catalysts were taken at a 4 $cm^{-1}$ of resolution.

## Acknowledgements

This work was supported by Grant-in-Aids from the Ministry of Education, Culture, Sports, Science and Technology (MEXT), Japan – "Elements Strategy Initiative to Form Core Research Center" program (since 2012), and by Grant-in-Aid for Scientific Research (B) (No. 15H04186). The authors thank Prof. Tsukasa Torimoto and Dr. Tatsuya Kameyama (Nagoya Univ.) for XRF measurement;

**Keywords:** Rhodium • nanoparticles • NO reduction • size effect • ensemble

[1] G. A. Somorjai, J. Y. Park, *Angew. Chem. Int. Ed.* **2008**, *47*, 9212-9228.

[2] a M. E. Grass, Y. Zhang, D. R. Butcher, J. Y. Park, Y. Li, H. Bluhm, K. M. Bratlie, T. Zhang, G. A. Somorjai, *Angew. Chem. Int. Ed.* **2008**, *47*, 8893-8896; b M. E. Grass, S. H. Joo, Y. Zhang, G. A. Somorjai, *J. Phys. Chem. C* **2009**, *113*, 8616-8623; c K. Qadir, S. H. Joo, B. S. Mun, D. R. Butcher, J. R. Renzas, F. Aksoy, Z. Liu, G. A. Somorjai, J. Y. Park, *Nano Lett.* **2012**, *12*, 5761; d D. A. J. M. Ligthart, R. A. van Santen, E. J. M. Hensen, *Angew. Chem. Int. Ed.* **2011**, *50*, 5306-5310; e S. H. Joo, J. Y. Park, J. R. Renzas, D. R. Butcher, W. Huang, G. A. Somorjai, *Nano Lett.* **2010**, *10*, 2709-2713.

[3] a N. Acerbi, S. C. E. Tsang, G. Jones, S. Golunski, P. Collier, *Angew. Chem. Int. Ed.* **2013**, *52*, 7737-7741; b M. Cargnello, V. V. T. Doan-Nguyen, T. R. Gordon, R. E. Diaz, E. A. Stach, R. J. Gorte, P. Fornasiero, C. B. Murray, *Science* **2013**, *341*, 771-773; c M. Machida, S. Minami, S. Hinokuma, H. Yoshida, Y. Nagao, T. Sato, Y. Nakahara, *J. Phys. Chem. C* **2015**, *119*, 373-380.

[4] a S. H. Oh, C. C. Eickel, *J. Catal.* **1991**, *128*, 526-536; b A. Miyazaki, I. Balint, Y. Nakano, *J. Nanopart. Res.* **2003**, *5*, 69-80; c P. Araya, F. Gracia, J. n. Cortés, E. E. Wolf, *Appl. Catal. B* **2002**, *38*, 77-90.

[5] R. Van Hardeveld, F. Hartog, *Surf. Sci.* **1969**, *15*, 189-230.

[6] a G. S. Herman, C. H. F. Peden, S. J. Schmieg, D. N. Belton, *Catal. Lett.* **1999**, *62*, 131-138; b L.-y. Huai, T. Su, H. Wen, X. Jin, J.-y. Liu, *J. Phys. Chem. C* **2016**, *120*, 5410-5419; c C. H. F. Peden, D. N. Belton, S. J. Schmieg, *J. Catal.* **1995**, *155*, 204-218; d K. Tian, X.-Y. Tu, S.-S. Dai, *Surf. Sci.* **2007**, *601*, 3186-3195.

[7] a Y. Mahara, H. Ishikawa, J. Ohyama, K. Sawabe, A. Satsuma, *Catal. Today* **2016**, *265*, 2-6; b Y. Mahara, H. Ishikawa, J. Ohyama, K. Sawabe, Y. Yamamoto, S. Arai, A. Satsuma, *Chem. Lett.* **2014**, *43*, 910-912; c Y. Mahara, J. Ohyama, T. Tojo, K. Murata, H. Ishikawa, A. Satsuma, *Catalysis Science & Technology* **2016**, *6*, 4773-4776; d Y. Mahara, T. Tojo, K. Murata, J. Ohyama, A. Satsuma, *RSC Adv.* **2017**, *7*, 34530-34537; e J. Ohyama, H. Ishikawa, Y. Mahara, T. Nishiyama, A. Satsuma, *Bull. Chem. Soc. Jpn.* **2016**, *89*, 914-921.

[8] a H. Hirai, Y. Nakao, N. Toshima, *J. Macromol. Sci. A* **1978**, *12*, 1117-1141; b T. Ashida, K. Miura, T. Nomoto, S. Yagi, H. Sumida, G. Kutluk, K. Soda, H. Namatame, M. Taniguchi, *Surf. Sci.* **2007**, *601*, 3898-3901.

[9] S. Bernal, F. J. Botana, J. J. Calvino, M. A. Cauqui, G. A. Cifredo, A. Jobacho, J. M. Pintado, J. M. Rodriguezizquierdo, *J. Phys. Chem.* **1993**, *97*, 4118-4123.

[10] a H. Permana, K. Y. Simon Ng, C. H. F. Peden, S. J. Schmieg, D. K. Lambert, D. N. Belton, *Catal. Lett.* **1997**, *47*, 5-15; b K. Almusaiteer, S. S. C. Chuang, *J. Catal.* **1998**, *180*, 161-170; c K. Almusaiteer, S. S. C. Chuang, *J. Catal.* **1999**, *184*, 189-201; d K. Almusaiteer, R. Krishnamurthy, S. S. C. Chuang, *Catal. Today* **2000**, *55*, 291-299; e T. I. Halkides, D. I. Kondarides, X. E. Verykios, *Catal. Today* **2002**, *73*, 213-221; f T. Tanabe, Y. Nagai, K. Dohmae, N. Takagi, N. Takahashi, S. i. Matsumoto, H. Shinjoh, *Appl. Catal. B* **2011**, *105*, 41-49.

[11] J. Stubenrauch, J. M. Vohs, *J. Catal.* **1996**, *159*, 50-57.

[12] J. Kašpar, C. de Leitenburg, P. Fornasiero, A. Trovarelli, M. Graziani, *J. Catal.* **1994**, *146*, 136-143.

[13] a D. I. Kondarides, Z. Zhang, X. E. Verykios, *J. Catal.* **1998**, *176*, 536-544; b S. Parres-Esclapez, I. Such-Basañez, M. J. Illán-Gómez, C. Salinas-Martínez de Lecea, A. Bueno-López, *J. Catal.* **2010**, *276*, 390-401; c P. Y. Sheng, W. W. Chiu, A. Yee, S. J. Morrison, H. Idriss, *Catal. Today* **2007**, *129*, 313-321; d J. Soria, A. Martinez-Arias, J. L. G. Fierro, J. C. Conesa, *Vacuum* **1995**, *46*, 1201-1204.

[14] M. P. Seah, W. A. Dench, *Surf. Interface Anal.* **1979**, *1*, 2-11.

[15] a K. A. Almusaiteer, S. S. C. Chuang, C.-D. Tan, *J. Catal.* **2000**, *189*, 247-252; b M. Haneda, T. Kaneko, N. Kamiuchi, M. Ozawa, *Catalysis Science & Technology* **2015**, *5*, 1792-1800; c J. T. Y. Jr., T. M. Duncan, S. D. Worley, R. W. Vaughan, *The Journal of Chemical Physics* **1979**, *70*, 1219-1224; d J. C. Matsubu, V. N. Yang, P. Christopher, *J. Am. Chem. Soc.* **2015**, *137*, 3076-3084; e V. Schwartz, A. Campos, A. Egbebi, J. J. Spivey, S. H. Overbury, *ACS Catal.* **2011**, *1*, 1298-1306; f F. Solymosi, M. Pasztor, *The Journal of Physical Chemistry* **1985**, *89*, 4789-4793; g G. Srinivas, S. S. C. Chuang, S. Debnath, *J. Catal.* **1994**, *148*, 748-758; h E. Varga, P. Pusztai, L. Ovari, A. Oszko, A. Erdohelyi, C. Papp, H. P. Steinruck, Z. Konya, J. Kiss, *PCCP* **2015**, *17*, 27154-27166; i A. J. McCue, G. A. Mutch, A. I. McNab, S. Campbell, J. A. Anderson, *Catal. Today* **2016**, *259*, 19-26; j P. B. Rasband, W. C. Hecker, *J. Catal.* **1993**, *139*, 551-560; k G. Srinivas, S. S. C. Chuang, *J. Catal.* **1993**, *144*, 131-147.

[16] B. E. Hayden, K. Kretzschmar, A. M. Bradshaw, R. G. Greenler, *Surf. Sci.* **1985**, *149*, 394-406.

[17] S. Misumi, H. Yoshida, S. Hinokuma, T. Sato, M. Machida, *Sci. Rep.* **2016**, *6*, 29737.

**Entry for the Table of Contents**

FULL PAPER

Size effect of $Rh/CeO_2$ on NO reduction under $NO\text{-}CO\text{-}C_3H_6\text{-}O_2$ at stoichiometric conditions was investigated. The turnover frequency (TOF) for NO reduction drastically increases according to their particle size due to Rh oxidation states. The variation of the TOF with Rh oxidation state suggested that Rh metal ensembles are highly active species for the NO reduction.

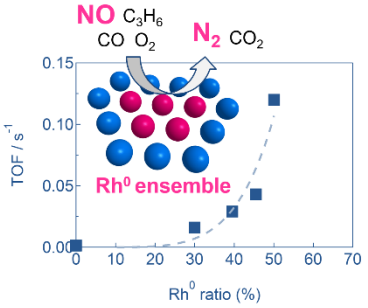


*Junya Ohyama,* Takumi Nishiyama, Atsushi Satsuma**

***Page No. – Page No.***

**Formation of Rh Metal Ensembles Facilitating NO Reduction over $Rh/CeO_2$ under Stoichiometric $NO\text{-}CO\text{-}C_3H_6\text{-}O_2$ Reaction**